Eur. Phys. J. D **33**, 193–199 (2005)
DOI: 10.1140/epjd/e2005-00046-4

THE EUROPEAN PHYSICAL JOURNAL D

Elastic and rotational excitation cross-sections for electron-water collisions in the low- and intermediate-energy ranges

L.E. Machado[1], L.M. Brescansin[2,a], I. Iga[3], and M.-T. Lee[3]

[1] Departamento de Física, UFSCar, 13565-905, São Carlos, SP, Brazil
[2] Instituto de Física Gleb Wataghin, UNICAMP, 13083-970, Campinas, SP, Brazil
[3] Departamento de Química, UFSCar, 13565-905, São Carlos, SP, Brazil

Received 28 September 2004
Published online 12 April 2005 –

Abstract. We present a theoretical study on electron-H_2O collisions in the low- and intermediate-energy ranges. More specifically, we report calculated elastic differential, integral and momentum transfer cross-sections as well as rotational excitation cross-sections in the (2–500)-eV range. In our calculations, an optical potential is used to represent the electron-molecule interaction. The Schwinger variational method combined with the distorted-wave approximation is used to solve the scattering equations. The comparison of our calculated results with other theoretical and/or experimental data available in the literature is very encouraging.

PACS. 34.80.Bm Elastic scattering of electrons by atoms and molecules

1 Introduction

Collisions of electrons with water molecules play an important role in a variety of research areas, such as atmospheric and interstellar processes, radiation biology, chemistry and plasma physics. For instance, it is well known that the water content of the human body is more than 70% by weight. The interaction of water molecules with secondary electrons of appreciable kinetic energy can lead to the formation of OH radicals [1], known as a carcinogenic agent [2,3]. Many investigations have been made on the deceleration and energy deposition of electrons in water [4,5]. Cross-sections for electron-gaseous water collisions are important in those studies, despite the possible difference in the electron interaction with gaseous or liquid water targets. Due to those important applications, electron scattering by water has been extensively studied for a long time. For example, a large amount of measurements of grand total (elastic + inelastic) cross-sections for this molecule has been performed since 1929 [6–10]. Also, experimental differential cross-sections (DCS) for elastic e^-–H_2O scattering have been reported in a wide incident energy range over the years [1,11–15]. Despite that, most of DCS measurements were carried out in a limited angular range, namely, between 10° to 150°. At larger scattering angles, DCS measurements are usually inaccessible due to the physical constraints of the electron spectrometers used. In 1996, Read and Channing [16] developed a magnetic angle-changing device which allowed the DCS for elastic electron-molecule scattering to be measured at angles up to 180°. This technique was recently used by Cho et al. [17] to determine absolute DCS for elastic electron scattering by water vapour in the 10–180° range.

On the theoretical side, the literature on elastic e^-–H_2O scattering is equally rich. Just to cite some, recent studies include calculations of cross-sections for rotationally resolved and/or unresolved elastic e^-–H_2O collisions of Machado et al. [18], Gianturco et al. [19], Varella et al. [20], and Faure et al. [21]. Despite that, most theoretical investigations on e^-–H_2O collisions have been performed at incident energies below 50 eV. Above this energy such investigations are scarce. A reliable theoretical study of the e^-–H_2O elastic scattering requires accurate descriptions for both short- and long-range interaction potentials. A fixed-nuclei treatment of electron scattering by polar molecules leads to divergent elastic DCS in the forward direction, due to the slow falloff of large partial-wave T-matrix elements [22]. This divergence can be removed only by the introduction of the nuclear motion in the Hamiltonian [23]. In addition, at intermediate incident energies, absorption effects would play an important role on electron-molecule interaction dynamics. Indeed, almost all inelastic channels are open, thus resulting in a reduction of the flux corresponding to the elastic channel. In this energy range, conventional close-coupling calculations of electron-molecule scattering would be an arduous computational task. Therefore, the use of model absorption potentials seems to be presently the only practical manner for treating electron-atom and electron-molecule

[a] e-mail: bresca@ifi.unicamp.br

collisions in this energy range. Several model absorption potentials have been proposed and used [24]. Among them, the version 3 of the quasi-free scattering model (QFSM), proposed by Staszewska et al. [25] and lately modified by Jain and Baluja [26], has shown to yield cross-sections in better agreement when compared with experiments. We have chosen this model to account for the absorption component of the electron-molecule interaction potential.

In this paper we perform a theoretical study on electron scattering by H_2O in the low- and intermediate-energy ranges. More specifically, elastic differential, integral (ICS), and momentum-transfer cross-sections (MTCS) as well as rotationally resolved cross-sections for electron scattering by H_2O are calculated in the (2–500)-eV range. A complex optical potential which includes static, exchange, correlation-polarization, and absorption contributions is used to represent the interaction dynamics, while a combination of the iterative Schwinger variational method (ISVM) [27] and the distorted-wave approximation (DWA) [28–30] is used to calculate accurate low-l partial-wave scattering. Rotationally elastic and inelastic cross-sections are calculated separately within the framework of the adiabatic-nuclei-rotation (ANR) approximation. Higher-angular-momentum dipole-potential components are then added up to infinity through a first Born approximation (FBA) closure formula. Rotationally unresolved cross-sections are obtained by summing up the rotationally elastic and inelastic contributions. Besides providing some new theoretical rotationally resolved and unresolved cross-sections for elastic electron scattering by H_2O, particularly at intermediate energies, the comparison of our calculated data with the newest experimental DCS of Cho et al. [17] would provide insights on the dynamics of backward scattering by polar molecules.

The organization of this paper is as follows: in Section 2, we describe briefly the theory used and also give some details of the calculation. In Section 3, we compare our calculated results with other theoretical and/or experimental data available in the literature and summarize our conclusions.

2 Theory and calculation

In this section we will briefly discuss the method used; details of the ISVM and DWA can be found elsewhere [27–30]. Within the ANR framework, the DCS for the excitation for an asymmetric-top rotor from an initial rotational level $J\tau$ to a final level $J'\tau'$ is given by

$$\frac{d\sigma}{d\Omega}(J\tau \longrightarrow J'\tau') = \frac{1}{(2J+1)}\frac{k_{J'\tau'}}{k_{J\tau}} \times \sum_{M=-J}^{J}\sum_{M'=-J'}^{J'} \left|f_{J\tau M \longrightarrow J'\tau' M'}\right|^2, \quad (1)$$

where $f_{J\tau M \longrightarrow J'\tau' M'}$ is the rotational excitation scattering amplitude related to the rotational eigenfunctions of the target by

$$f_{J\tau M \longrightarrow J'\tau' M'} = \langle \Psi_{J'\tau' M'}(\Omega) \mid f^{LF} \mid \Psi_{J\tau M}(\Omega)\rangle, \quad (2)$$

$k_{J\tau}$ and $k_{J'\tau'}$ are the magnitudes of the linear momenta of the incident and the scattered electrons, respectively, and $\Omega \equiv (\alpha, \beta, \gamma)$ are the Euler angles defining the frame transformation [31]. The eigenfunctions $\Psi_{J\tau M}(\Omega)$ appearing in equation (2) are written as linear combinations of symmetric-top eigenfunctions [32]:

$$\Psi_{J\tau M}(\Omega) = \sum_{K=-J}^{J} a_{KM}^{J\tau} \Phi_{JKM}(\Omega), \quad (3)$$

where the symmetric-top eigenfunctions are given by

$$\Phi_{JKM}(\Omega) = \left(\frac{2J+1}{8\pi^2}\right) D_{KM}^{J^*}(\Omega), \quad (4)$$

where D_{KM}^{J} are the well-known Wigner rotation matrices [31]. Also, f^{LF} appearing in equation (2) is the electronic part of the laboratory-frame scattering amplitude which can be related to the corresponding body-frame T-matrix by an usual frame transformation. The latter can be conveniently partial-wave expanded as

$$T = \frac{1}{k}\sum_{p\mu l h l' h'} i^{l-l'} T^{p\mu}_{k,lh;l'h'} X^{p\mu}_{lh}(\hat{k}) X^{p\mu^*}_{l'h'}(\hat{k}_0) \quad (5)$$

where $\hat{k}_0$ and $\hat{k}$ are the linear momentum directions of the incident and scattered electrons in BF, respectively, and $X^{p\mu}_{lh}(\hat{k})$ are the symmetry-adapted functions [33] which are expanded in terms of the usual spherical harmonics as follows:

$$X^{p\mu}_{lh}(\hat{r}) = \sum_{m} b^{p\mu}_{lhm} Y_{lm}(\hat{r}). \quad (6)$$

Here p is an irreducible representation (IR) of the molecular point group, μ is a component of this representation and h distinguishes between different bases of the same IR corresponding to the same value of l. The coefficients $b^{p\mu}_{lhm}$ satisfy important orthogonality relations and are tabulated for C_{2v} and O_h point groups [33].

In the present study, the electron-molecule scattering dynamics is represented by an interaction potential given by

$$V(\boldsymbol{r}) = V^{SEP} + iV_{ab}, \quad (7)$$

with

$$V^{SEP} = V_{st} + V_{ex} + V_{cp}, \quad (8)$$

where V_{st}, V_{ex}, and V_{cp} are the static, the exchange, and the correlation-polarization contributions, respectively. In our calculation, V_{st} and V_{ex} are derived exactly from a Hartree-Fock SCF target wavefunction. In this work, an SCF wavefunction for the ground state of H_2O is constructed with a $[9s5p/3s2p]$ contracted Cartesian Gaussian basis set of Dunning [34] augmented by one d ($\alpha = 0.34$) uncontracted function centered on the oxygen atom and a $[4s/2s]$ contracted set for hydrogen [35]. With this basis set, our calculated electric dipole moment at the experimental equilibrium geometry is 0.762 a.u., which can be compared with the calculated value 0.780 a.u. of

Gianturco et al. [19]. The experimental dipole moment is 0.724 a.u. [36].

A parameter-free model potential introduced by Padial and Norcross [37] is used to account for the correlation-polarization contributions. In this model, a short-range correlation potential between the scattering and the target electrons is defined in an inner interaction region and a long-range polarization potential in an outer region. The correlation potential is calculated by a free-electron-gas model, derived using the target electronic density according to equation (9) of Padial and Norcross [37]. In addition, an asymptotic form of the polarization potential is used for the long-range electron-target interaction. The theoretical values $\alpha_{00} = 10.625$ a.u., $\alpha_{20} = -0.636$ a.u., and $\alpha_{22} = 0.308$ a.u. of the polarizability components were used to calculate the asymptotic form of V_{cp}. Our calculated spherical polarizability α_{00} is in good agreement with the experimental value of 11.0 a.u. [39]. The first crossing of the correlation and polarization potential curves defines the inner and the outer region. No cut-off or other adjusted parameters are needed for the calculation of V_{cp}. As stated before, the absorption potential V_{ab} in equation (7) is taken as the modified version [26] of the quasi-free scattering model, derived by Staszewska et al. [25].

In the present study, we have limited the partial-wave expansion of the T-matrix elements up to $l_{max} = 16$ and $m_{max} = 16$. Since H_2O is a polar molecule, these partial-wave expansions converge slowly due to the long-range dipole interaction potential. Therefore, a Born-closure formula is used to account for the contribution of higher partial-wave components to the scattering amplitudes. Accordingly, equation (5) is rewritten as

$$T = T^B + \frac{1}{k} \sum_{p\mu l h l' h'}^{LL'} i^{l-l'} \left(T^{p\mu\,ISVM}_{k,lh;l'h'} - T^{p\mu\,B}_{k,lh;l'h'} \right) \times X^{p\mu}_{lh}(\hat{k}) X^{p\mu\,*}_{l'h'}(\hat{k}_0) \quad (9)$$

where T^B is the complete point-dipole FBA T-matrix, $T^{p\mu\,ISVM}_{k,lh;l'h'}$ are the partial-wave T-matrix elements calculated via ISVM and $T^{p\mu\,B}_{k,lh;l'h'}$ are the corresponding partial-wave point-dipole FBA T-matrix elements, given by

$$T^{p\mu\,B}_{k,lh;l'h'} = -\frac{D}{L} \left[\frac{(L+h)(L-h)}{(2L+1)(2L-1)} \right]^{\frac{1}{2}}, \quad (10)$$

where D is the target electric dipole moment and $L = l'$ when $l' = l + 1$ and $L = l$ when $l' = l - 1$.

3 Results and discussion

In Figures 1–4, we compare our calculated DCS (rotationally summed) with the existing measured data [1,13–15,17] for elastic e^-–H_2O scattering in the incident energy range of 2–500 eV. Some recent theoretical results available in the literature [19–21,38] are also shown

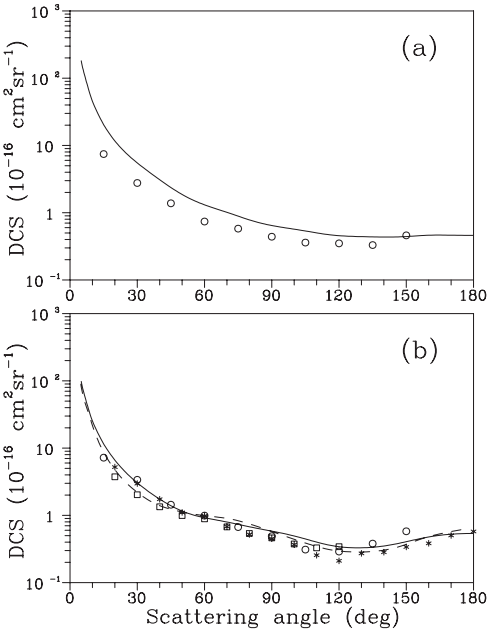

Fig. 1. DCS for elastic e^-–H_2O scattering at the impact energy of (a) 2 eV and (b) 4 eV. Solid line, present rotationally summed results; dashed line, theoretical results of Faure et al. [21]; open squares, experimental results of Danjo and Nishimura [13]; open circles, experimental data of Shyn and Cho [14]; asterisks, experimental results of Cho et al. [17].

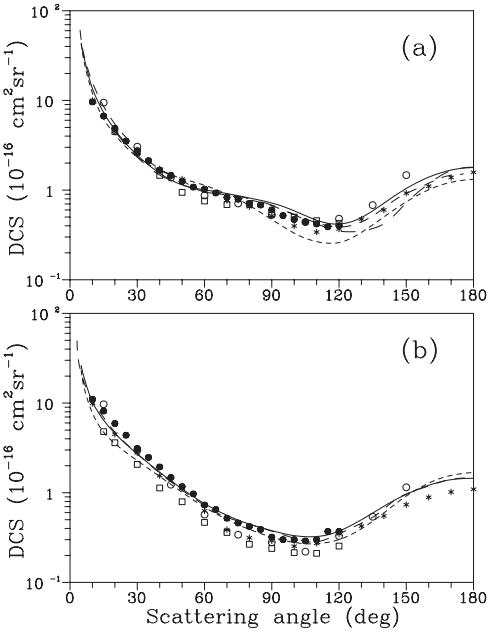

Fig. 2. Same as Figure 1 but for (a) 10 eV and (b) 20 eV. The symbols are the same as in Figure 1, except: short-dashed line, calculated results of Varella et al. [20]; dashed line, theoretical results of Gianturco et al. [19]; long-dashed line, calculated results of Greer and Thompson [38]; full circles, experimental results of Johnstone and Newell [15].

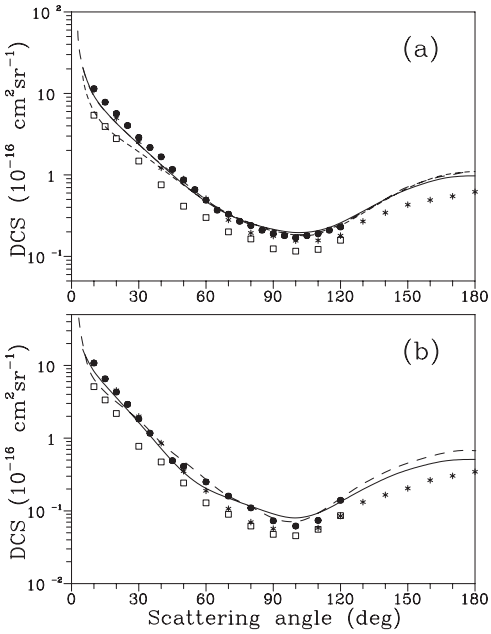

Fig. 3. Same as Figure 2 but for (a) 30 eV and (b) 50 eV.

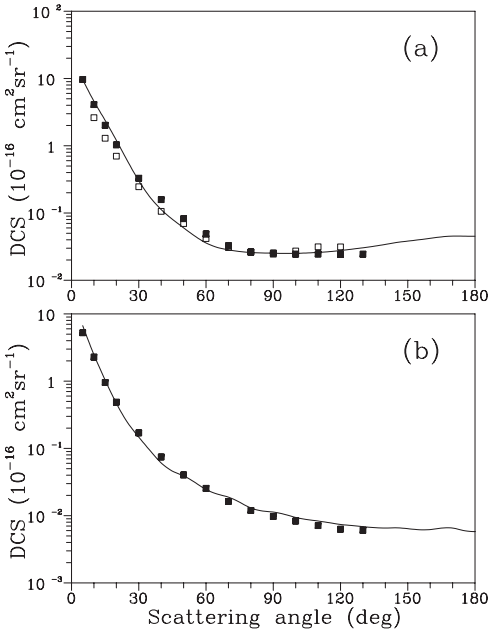

Fig. 4. Same as Figure 2 but for (a) 200 eV and (b) 500 eV, except: full squares, experimental results of Katase et al. [1].

for comparison. For all energies studied herein, our calculated results agree quite well with most of the experimental data, both in shape and magnitude. Particularly, our calculation has predicted correctly the backward scattering behavior of the DCS, when compared with the recent experimental data of Cho et al. [17]. Moreover, the sharp increase of the DCS at small scattering angles, due to the polar nature of the target, is also well described by our

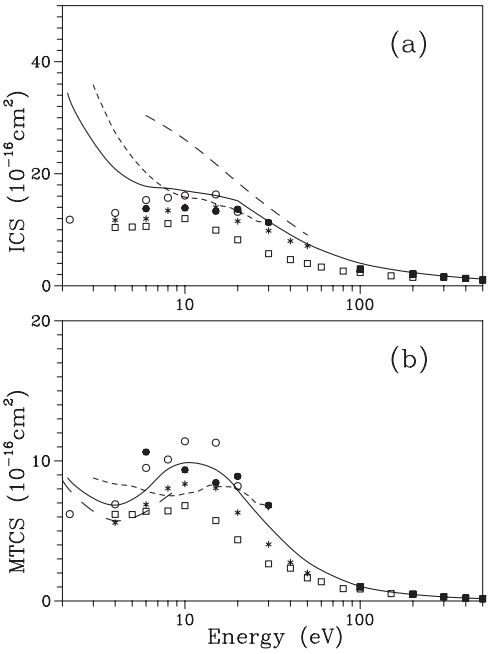

Fig. 5. Rotationally summed (a) ICS and (b) MTCS for elastic e^-–H_2O scattering. Solid line, present calculated results; short-dashed line, calculated results of Varella et al. [20]; dashed line, theoretical results of Gianturco et al. [19]; long-dashed line, calculated results of Greer and Thompson [38]; full circles, experimental results of Johnstone and Newell [15]; open circles, experimental results of Shyn and Cho [14]; open squares, experimental results of Danjo and Nishimura [13]; full squares, experimental results of Katase et al. [1]; asterisks, experimental results of Cho et al. [17].

calculation. General good agreement is observed as well between our results and other existing theoretical results.

Figures 5a and 5b show our calculated elastic ICS and MTCS, respectively, in the (2–500)-eV range, along with the experimental [1,13–15,17] and theoretical results [19,20,38] available in the literature. In general, both our calculated ICS and MTCS agree well with the experimental data of Johnstone and Newell [15], Shyn and Cho [14], and Cho et al. [17] at incident energies in the (5–50)-eV range, and with those of Katase et al. [1] in the (100–500)-eV range. At lower energies, all experimental ICS lie well below the theoretical predictions, probably due to difficulties in the extrapolation procedure near the forward direction, where the DCS contribute significantly to the ICS, particularly for strongly polar targets. On the other hand, the experimental data of Danjo and Nishimura [13] lie systematically below our data for incident energies below 100 eV. Comparing with other theoretical studies, our ICS agree quite well with the calculated results of Varella et al. [20] in the (8–30)-eV range. Nevertheless, the ICS calculated by Gianturco et al. [19] are substantially higher than our data. In Figure 5b, our MTCS agree well with those of Greer and Thompson [38]. At low energies, our MTCS also indicate a sharp increase towards the zero incident energy, reflecting the polar

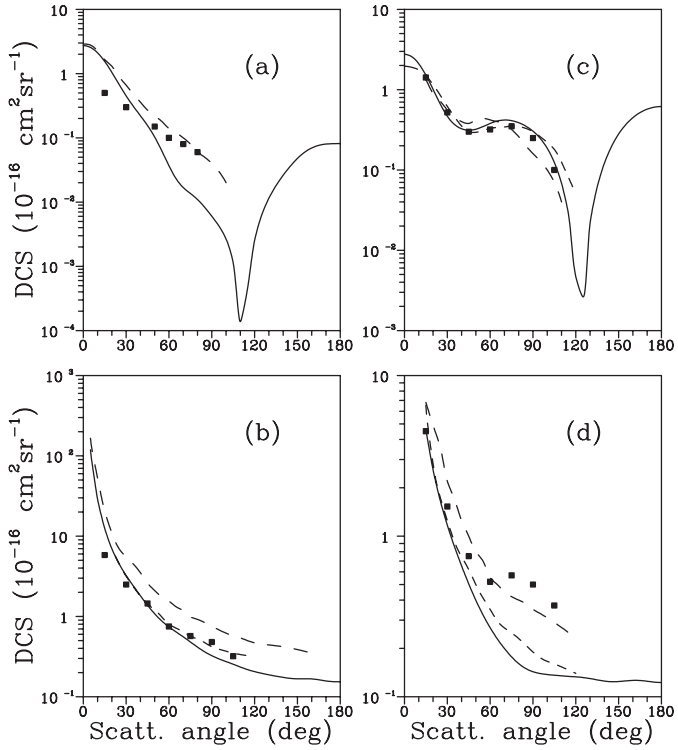

Fig. 6. Rotationally resolved DCS for e^-–H_2O scattering for (a) the (0→0) elastic process and (b) the averaged $\frac{1}{2}[(0\rightarrow1)+(1\rightarrow0)]$ rotational excitation/de-excitation process, both at 2.14 eV, and for (c) the (0→0) elastic process and (d) the averaged $\frac{1}{2}[(0\rightarrow1)+(1\rightarrow0)]$ rotational excitation/de-excitation process, both at 6 eV. Solid line, present results; dashed lines, theoretical results of Gianturco et al. [19]; long-dashed lines, theoretical results of Jain and Thompson [40]; full squares, experimental results of Jung et al. [12].

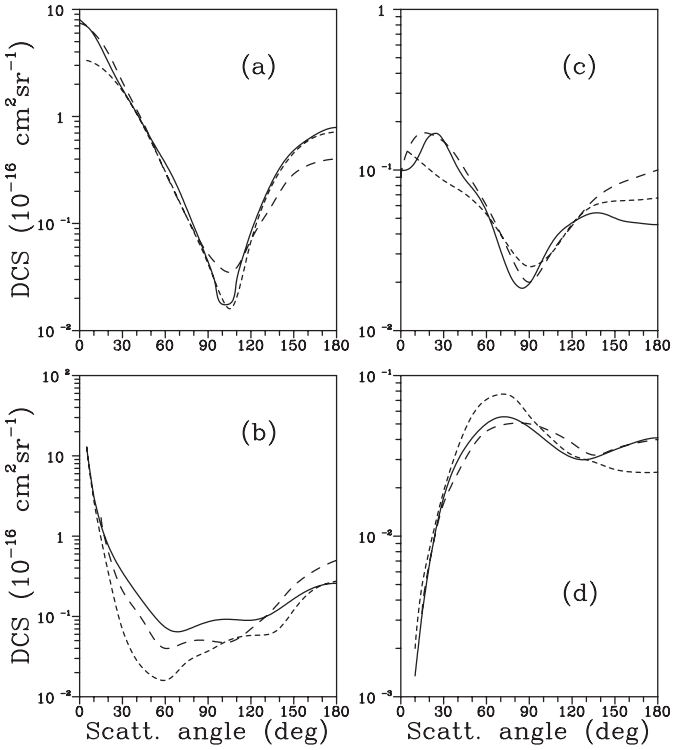

Fig. 7. Rotationally resolved DCS for e^-–H_2O scattering at 30 eV for rotational (a) (0→0), (0→1), (c) (0→2), and (d) (0→3) transitions. Solid line, present results; short-dashed lines, theoretical results of Varella et al. [41]; dashed line, calculated results of Gianturco et al. [19].

nature of the target. Similar behavior is also seen in the calculated data of Greer and Thompson [38]. On the other hand, the energy dependence of the calculated MTCS of Varella et al. [20] is relatively flat in the (3–30)-eV range.

Figures 6a and 6b show our results for the rotationally elastic and the averaged $\frac{1}{2}[(0\rightarrow1)+(1\rightarrow0)]$ rotational excitation/de-excitation DCS at 2.14 eV, respectively, along with the experimental results of Jung et al. [12] and the available theoretical results of Jain and Thompson [40] and Gianturco et al. [19]. Similar comparison, but for 6 eV, is shown in Figures 6c and 6d. Our results agree reasonably well with the experimental and other theoretical results, although none of the calculations was able to predict the broad maximum centered at around 70° seen in the experimental data of Figure 6d. Since the results of three different calculations agree reasonably well with each other at least qualitatively, we think that new measurements would be needed to confirm or to disprove that structure.

Figures 7a–7d show our DCS for the $(0\rightarrow0,1,2,3)$ rotational transitions, respectively, at 30 eV. Unfortunately, there are no experimental results available in the literature. Therefore, comparison is made only with other calculated data [41,19]. A general overall agreement is observed among all the calculated results.

In Figures 8a and 8b we present our calculated DCS for the $(0\rightarrow0,1,2,3)$ rotational transitions at 80 and 200 eV, respectively. Also in these cases, no results are available in the literature for comparison. In general, the $(0\rightarrow0,1)$ transitions are dominant. Also, the DCS become more oscillatory with increasing incident energies.

Finally, Figures 9a–9d show our calculated ICS for the $(0\rightarrow0,1,2,3)$ rotational transitions, respectively, in the (2–500)-eV energy range. Again, theoretical results of Varella et al. [41] and Gianturco et al. [19] are presented for comparison. For the (0→0) rotational transition, our calculated data agree very well with those of Gianturco et al. [19]. On the other hand, the calculated results of Varella et al. [41] lie significantly above our data for energies below 7 eV. In contrast, for the (0→1) transition, our calculated data agree very well with those of Varella et al. [41], whereas the results of Gianturco et al. [19] are significantly larger in the entire energy range. For $(0\rightarrow2,3)$ transitions, the agreement between the present results and those of Gianturco et al. [19] is very good. Again, discrepancies are observed when compared with the calculation of Varella et al. [41] at lower-end energies. In particular, the additional maximum located at around 2.5 eV in their ICS for the (0→3) rotational transition is not reproduced in our study. The reason for such discrepancy is unclear.

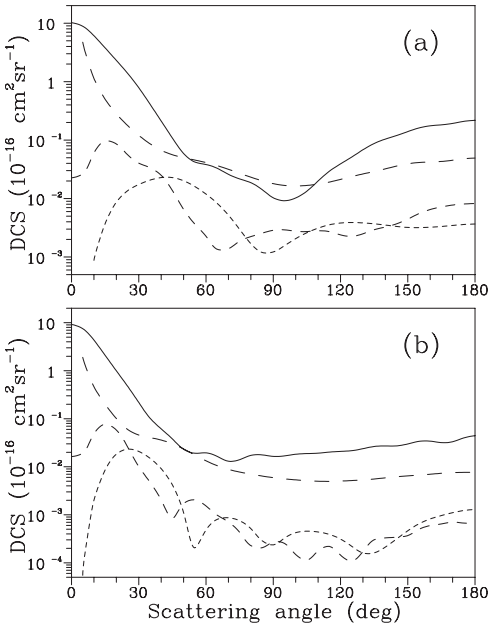

Fig. 8. Rotationally resolved DCS for e^-–H_2O scattering at (a) 80 eV and (b) 200 eV. Solid line, 0→0 transition; long-dashed line, 0→1 transition; dashed line, 0→2 transition; short-dashed line, 0→3 transition.

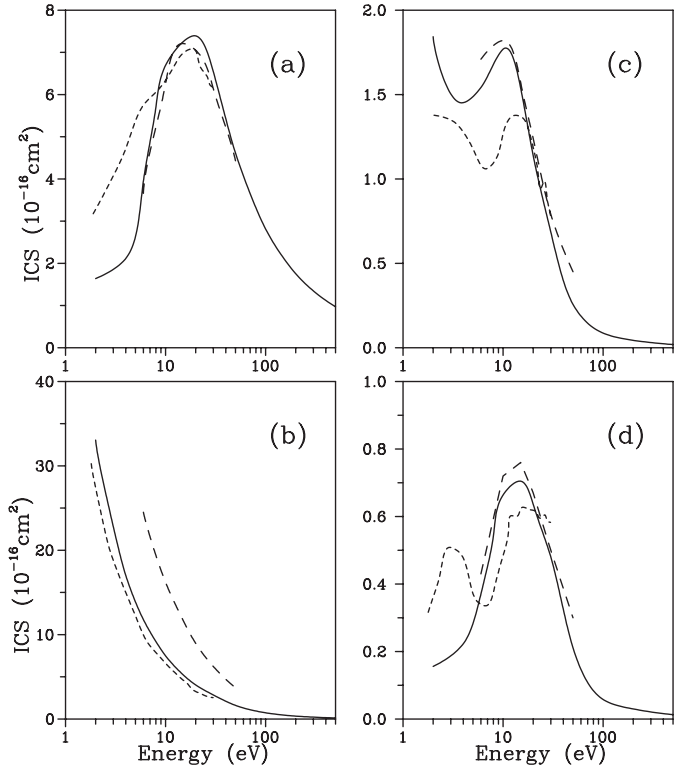

Fig. 9. Rotationally resolved ICS for e^-–H_2O scattering. (a) 0→0 transition, (b) 0→1 transition; (c) 0→2 transition; (d) 0→3 transition. Solid line, present calculated results; dashed line, calculated results of Gianturco et al. [19]; short-dashed line, theoretical results of Varella et al. [41].

In summary, we performed a theoretical study on e^-–H_2O scattering in the low- and intermediate-energy ranges. Despite the simplicity of the interaction dynamics used, the comparison with the experimental and theoretical results available in the literature has shown that our method is able to provide reliable elastic and rotational excitation cross-sections in a wide energy range. In particular, the backward scattering behavior of the DCS recently observed by Cho et al. is also well described by our calculations.

This research was partially supported by the Brazilian agencies CNPq and FAPESP.

References

1. A. Katase, K. Ishibashi, Y. Matsumoto, T. Sakae, S. Maezono, E. Murakami, K. Watanabe, H. Maki, J. Phys. B: At. Mol. Opt. Phys. **19**, 2715 (1986)
2. E. Fernandes, S.A. Toste, J.L.F.C. Lima, S.J. Reis, Free Radical Bio. Med. **35**, 1008 (2003)
3. H.B. An, J. Xie, J.Q. Zhao, Z.S. Li, Free Radical Res. **37**, 1107 (2003)
4. J.E. Turner, H. Peretzke, R.N. Hamm, H.A. Wright, R.H. Ritchie, Radiat. Res. **9**, 47 (1982)
5. J.E. Turner, J.L. Magee, H.A. Wright, A. Chattergee, R.N. Hamm, R.H. Ritchie, Radiat. Res. **96**, 437 (1983)
6. E. Brüche, Ann. Phys. Lpz. **1**, 93 (1929)
7. V.F. Sokolov, Y.A. Sokolova, Sov. Tech. Phys. Lett. **7**, 268 (1981)
8. C. Szmytkowski, Chem. Phys. Lett. **136**, 363 (1987)
9. A. Zecca, G. Karwasz, S. Oss, R. Grisenti, R.S. Brusa, J. Phys. B: At. Mol. Opt. Phys. **20**, L133 (1987)
10. Z. Sağlam, N. Aktekin, J. Phys. B: At. Mol. Opt. Phys. **23**, 1529 (1990)
11. S. Trajmar, W. William, A. Kuppermann, J. Chem. Phys. **58**, 2521 (1973)
12. K. Jung, Th. Antoni, R. Müller, K.-H. Kochem, H. Ehrhardt, J. Phys. B: At. Mol. Opt. Phys. **15**, 3535 (1982)
13. A. Danjo, H. Nishimura, J. Phys. Soc. Jap. **54**, 1224 (1985)
14. T.W. Shyn, S.Y. Cho, Phys. Rev. A **36**, 5138 (1987)
15. W.M. Johnstone, W.R. Newell, J. Phys. B: At. Mol. Opt. Phys. **24**, 3633 (1991)
16. F.H. Read, J.N. Channing, Rev. Sci. Instrum. **67**, 2372 (1996)
17. H. Cho, Y.S. Park, H. Tanaka, S.J. Buckman, J. Phys. B: At. Mol. Opt. Phys. **37**, 625 (2004)
18. L.E. Machado, L. Mu-Tao, L.M. Brescansin, M.A. Lima, V. McKoy, J. Phys. B: At. Mol. Opt. Phys. **28**, 467 (1995)
19. F.A. Gianturco, S. Meloni, P. Paioletti, R.R. Lucchese, N. Sanna, J. Chem. Phys. **108**, 4002 (1998)
20. M.T. do N. Varella, M.H.F. Bettega, M.A.P. Lima, L.G. Ferreira, J. Chem. Phys. **111**, 6396 (1999)
21. A. Faure, J.D. Gorfinkiel, J. Tennyson, J. Phys. B: At. Mol. Opt. Phys. **37**, 801 (2004)
22. D.W. Norcross, L.A. Collins, Adv. At. Mol. Phys. **18**, 341 (1982)
23. T.N. Rescigno, A.E. Orel, A.U. Hazi, B.V. McKoy, Phys. Rev. A **26**, 690 (1982)
24. M.-T Lee, I. Iga, L.E. Machado, L.M. Brescansin, Phys. Rev. A **62**, 062710 (2000)

25. G. Staszewska, D.W. Schwenke, D.G. Truhlar, Phys. Rev. A **29**, 3078 (1984)
26. A. Jain, K.L. Baluja, Phys. Rev. A **45**, 202 (1992)
27. R.R. Lucchese, G. Raseev, V. McKoy, Phys. Rev. A **25**, 2572 (1982)
28. A.W. Fliflet, V. McKoy, Phys. Rev. A **21**, 1863 (1980)
29. M.-T. Lee, V. McKoy, Phys. Rev. A **28**, 697 (1983)
30. M.-T. Lee, S. Michelin, L.E. Machado, L.M. Brescansin, J. Phys. B: At. Mol. Opt. Phys. **26**, L203 (1993)
31. M.E. Rose, *Elementary Theory of Angular Momentum* (John Wiley, N.Y., 1957)
32. A. Jain, D.G. Thompson, Comput. Phys. Commun. **30**, 301 (1983)
33. P.G. Burke, N. Chandra, F.A. Gianturco, J. Phys. B: At. Mol. Opt. Phys. **5**, 2212 (1972)
34. T.H. Dunning Jr, J. Chem. Phys. **53**, 2823 (1970)
35. T.H. Dunning Jr, R.M. Pitzer, S. Aung, J. Chem. Phys. **57**, 5051 (1972)
36. W. Meyer, in *Modern Theoretical Chemistry*, edited by H.F. Schaefer III (Press, New York, 1977), Vol. 3, p. 442
37. N.T. Padial, D.W. Norcross, Phys. Rev. A **29**, 1742 (1984)
38. R. Greer, D.G. Thompson, J. Phys. B: At. Mol. Opt. Phys. **27**, 3533 (1994)
39. J.O. Hirschfelder, C.F. Curtis, R.B. Bird, *Molecular Theory of Gases and Liquids* (John Willey, N.Y., 1954)
40. A. Jain, D.G. Thompson, J. Phys. B: At. Mol. Opt. Phys. **16**, 3077 (1983)
41. M.T. do N. Varella, M.H.F. Bettega, A.P.P. Natalense, L.G. Ferreira, M.A.P. Lima, Braz. J. Phys. **31**, 21 (2001)